1 **Dynamic response and breakage of trees subject to a landslide-induced air blast**

2 Yu Zhuang[1,2], Aiguo Xing[1], Perry Bartelt[3], Muhammad Bilal[1], Zhaowei Ding[2]

3 [1]State Key Laboratory of Ocean Engineering, Shanghai Jiao Tong University, Shanghai, 200240, PR China

4 [2]State Key Laboratory of Geohazard Prevention and Geoenvironment Protection, Chengdu University of

5 Technology, Chengdu, 610059, China

6 [3]WSL Institute for Snow and Avalanche Research SLF, Flüelastrasse 11, 7260 Davos Dorf, Switzerland

7 Correspondence: Aiguo Xing (xingaiguo@sjtu.edu.cn)

9 **Abstract**

10 Landslides have been known to generate powerful air blasts capable of causing destruction and casualties

11 far beyond the runout of sliding mass. The extent of tree damage provides valuable information on air

12 blast intensity and impact region. However, little attention has been paid to the air blast-tree interaction.

13 In this study, we proposed a framework to assess the tree destruction caused by powerful air blasts,

14 including the eigenfrequency prediction method, tree motion equations and the breakage conditions. The

15 tree is modeled as a flexible beam with variable cross-sections, and the anchorage stiffness is introduced

16 to describe the tilt of tree base. Large tree deflection is regarded when calculating the air blast loading,

17 and two failure modes (bending and overturning) and the associated failure criteria are defined. Modeling

18 results indicate that although the anchorage properties are of importance to the tree eigenfrequency, tree

19 eigenfrequency is always close to the air blast frequency, causing a dynamic magnification effect for the

20 tree deformation. This magnification effect is significant in cases with a low air blast velocity, while the

21 large tree deflection caused by strong air blast loading would weaken this effect. Furthermore, failure

22 modes of a specific forest subject to a powerful air blast depend heavily on the trunk bending strength

and anchorage characteristics. The large variation of biometric and mechanical properties of trees necessitates the establishment of a regional database of tree parameters. Our work and the proposed method are expected to make people better understand air blast power and be of great utility for air blast risk assessment in mountainous regions worldwide.

Keywords: Landslide-induced air blast; Tree eigenfrequency; Dynamic response; Tree breakage

1 Introduction

Long runout landslides involve massive amounts of energy and can be extremely hazardous owing to their long movement distance, high mobility and potential chain disasters (Johnson and Campbell, 2017; Shugar et al., 2021). A moving landslide with high velocity can generate a powerful air blast capable of uprooting trees, lifting people into the air and even flattening buildings (Adams, 1881; Penna et al., 2021). In recent decades, destructive air blasts frequently occurred in mountainous regions worldwide and caused casualties and economic loss far beyond the landslide runout (e.g., Yin, 2014; Bartelt et al., 2016; Kargel et al., 2016). Understanding their force of destruction is of great utility for landslide risk assessment and disaster mitigation in high-altitude regions.

Monitoring equipment has been confirmed to provide great performance in determining the dynamic characteristics of landslide-induced air blasts (Grigoryan et al., 1982; Sukhanov, 1982; Caviezel et al., 2021). However, most case histories occurred in the high-altitude mountainous region without witnesses (Yin and Xing, 2012), and the in-situ equipment can also get damaged because of the near-field destruction of landslides and associated air blasts. Therefore, very few air blast cases were measured in history. Geologists can only evaluate the air blast hazard for most recorded events using historical evidence after the landslide occurred. In-situ information about forest destruction and tree breakage is often used for the air blast risk assessment (Feistl et al., 2015; Fujita et al., 2017; Zhuang et al., 2019,

45   2022a) (Fig. 1). Uprooted trees and snapped stems delineate the impact region of air blasts and create a

46   natural vector field indicating the primary movement direction of the landslide, greatly helping analyze

47   the disaster-causing process of the event. In many cases, observations of forest destruction are the only

48   data to quantify air blast danger.

49

50   **Fig. 1** Trees breakage caused by a large landslide-induced air blast in Sichuan, China, 2008.

51   A question remained for air blast mitigation planning using the information of tree damage is how

52   to establish a simple relationship between air blast impact pressure and tree failure. Bending and

53   overturning are two common tree failure modes caused by strong winds. Trees snap when the bending

54   stress exerted by the air blast exceeds the wood strength (Peltola et al., 1999; Gardiner et al., 2000), while

55   the overturning will occur if the applied moment overcomes the anchorage resistance of root systems

56   (Jonsson et al., 2006; Nicoll et al., 2006). The occurrence of these two failure modes depends heavily on

57   both the air blast loading and tree properties. Considering the minor destruction of air blasts relative to

58   the landslide, although long recognized that sliding mass can easily break or uproot trees (Bartelt and

59   Stöckli, 2001; Šilhán, 2020), little attention has been paid to the tree destruction resulting from air blasts.

60   Furthermore, existing models describing the tree-air blast interaction are mostly static (Feistl et al., 2015)

61   or established based on the small-deflection theory (Bartelt et al., 2018). These methods could aid in a

62   rapid assessment of air blast power, but further research is needed to establish a dynamic model to

63   represent the dynamic response of trees in a strong wind. A mechanical understanding of how trees are

64   damaged by air blasts is therefore essential for quantifying the air blast powers and providing valuable

65   data to verify the possible numerical results.

66   In this study, we established a simple dynamic model capable of calculating the natural frequency

67   of trees and simulating their dynamic response subject to a powerful air blast. The proposed model

68   regards the tree as a multi-degree-of-freedom beam with variable diameters and accounts for large tree

69   deflections and impacts of root anchorage. Both bending and overturning failure modes are involved in

70   the model. The work conducted in this study is expected to make people better understand the power of

71   landslide-induced air blasts and provide an applicable method to assess the air blast hazard.

72   **2. Model description**

73   Measurements of historical events indicated that the landslide-induced air blast is intermittent and of

74   short duration, lasting only a few seconds and could reach a high velocity (Grigoryan et al., 1982;

75   Sukhanov, 1982; Caviezel et al., 2021). This impulse wave has a propagation distance of hundreds of

76   meters in both horizontal and vertical directions and acts over the entire tree. Thus, the impact of air

77   blasts on trees is similar to extreme wind gusts, producing large bending moments in the stem and root

78   base system, forcing trees to deform or get damaged. Furthermore, fallen trees often point to the

79   movement direction of the landslide, illustrating there is little time for trees to sway and react to air blasts

80   while the inertial effects are greatly important.

81   To characterize the dynamic response of trees under the impact load of air blasts, we established a

82   mechanical model to predict the eigenfrequency of trees subject to air blasts and developed a dynamic

83   tree-swaying model that accounts for the large tree deflection. In what follows, we present the

84   eigenfrequency prediction method, tree motion equations and the breakage conditions.

85   *2.1 Eigenfrequency prediction*

86   The tree is modeled as a flexible cantilever beam with variable diameters that is hinged at ground level

87   using elastic support. The beam diameter is assumed to continuously linearly decrease with height

88   regarding the decreasing diameters of trunk and crown from bottom to top, while the anchorage stiffness

89   of the root system (K) helps to describe the tilt of tree base in response to the moment (Neild and Wood,

90   1999). In the eigenfrequency prediction mode, the tree beam is divided into two segments with a splitting

91   point located at the starting point of the tree crown (Fig. 2). We assume that the tree crown shows minor

92   impacts on elastic modulus. The tree crown is accounted for through the crown mass, and thus the natural

93   difference between the two segments is the material density.

94   The governing differential equation for the dynamic bending of a nonuniform Euler-Bernoulli beam

95   is (Keshmiri et al., 2018):

96
$$\rho A(z)\frac{\partial^2 u}{\partial t^2} + \frac{\partial^2 u}{\partial z^2}\left[EI(z)\frac{\partial^2 u}{\partial z^2}\right] = 0 \tag{1}$$

97   where z is the position variable along the beam length. For ease of calculation, the original point ($z=0$) is

98   set at the treetop and the maximum value of z is at the tree base, so that the beam diameter $d(z)$

99   corresponding to the position z can be described using a gradient coefficient (μ): $d(z)=\mu z$. u is the beam

100   displacement, E is the elastic modulus, $A(z) = \frac{\pi}{4}(dz)^2$ and $I(z) = \frac{\pi}{64}(dz)^4$ are the cross-sectional area

101   and moment of inertia, respectively.

102
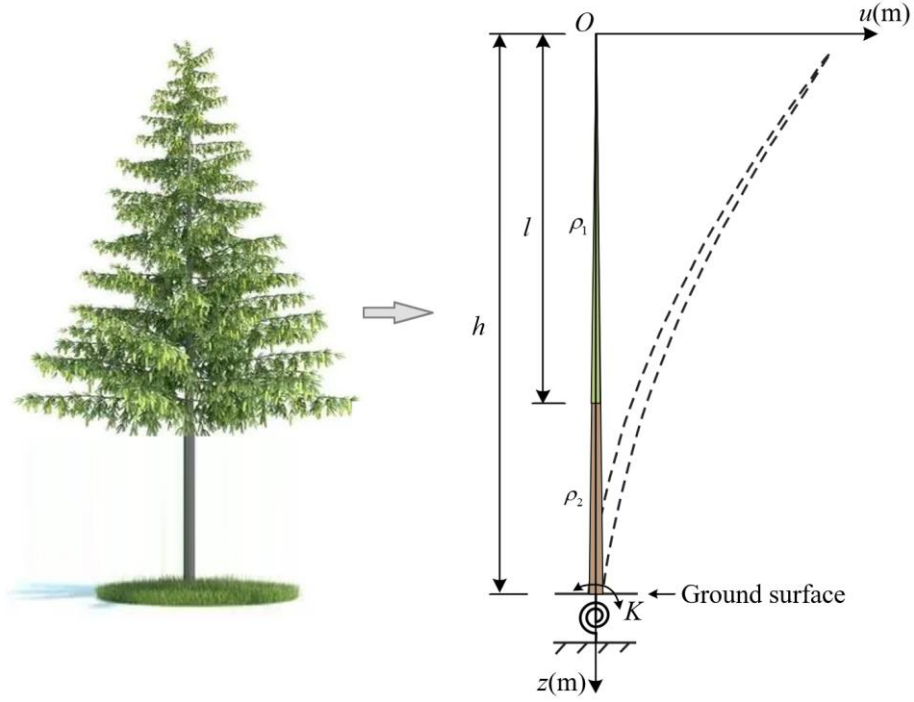
103   **Fig. 2** Schematic representation of the eigenfrequency prediction model.

104   Plugging the expression of $A(z)$ and $I(z)$ into Eq. 1 gives:

105
$$z^2 \frac{\partial^4 u}{\partial z^4} + 8z \frac{\partial^3 u}{\partial z^3} + 12 \frac{\partial^2 u}{\partial z^2} - \frac{16\rho\omega^2 u}{E\mu^2} = 0 \qquad (2)$$

106   where ω is known as the eigenfrequency of the beam. The general solution of Eq. 2 can be expressed as:

107
$$u(z) = \frac{1}{z}\left[A_1 J_2(2\sqrt{\lambda z}) + A_2 Y_2(2\sqrt{\lambda z}) + A_3 J_2(2i\sqrt{\lambda z}) + A_4 Y_2(2i\sqrt{\lambda z}) \right] \qquad (3)$$

108   where $\lambda = \sqrt{\dfrac{16\rho\omega^2}{E\mu^2}}$, J_2 and Y_2 are the Bessel functions of the first and second kind (Mocica, 1988),

109   respectively, and A_1-A_4 are coefficients that need to be determined based on the boundary conditions.

110   The deflection of the upper segment (crown) and the lower segment (trunk) can be generated in a

111   similar manner:

112
$$u_1(z) = \frac{1}{z}\left[A_1 J_2\left(2\sqrt{\lambda_1 z}\right) + A_2 Y_2\left(2\sqrt{\lambda_1 z}\right) + A_3 J_2\left(2i\sqrt{\lambda_1 z}\right) + A_4 Y_2\left(2i\sqrt{\lambda_1 z}\right) \right] \quad 0 \leqslant z < l \quad (4)$$

113
$$u_2(z) = \frac{1}{z}\left[B_1 J_2\left(2\sqrt{\lambda_2 z}\right) + B_2 Y_2\left(2\sqrt{\lambda_2 z}\right) + B_3 J_2\left(2i\sqrt{\lambda_2 z}\right) + B_4 Y_2\left(2i\sqrt{\lambda_2 z}\right) \right] \quad l \leqslant z \leqslant h \quad (5)$$

114   where l is the length of crown, h is the tree height, $\lambda_1 = \sqrt{\dfrac{16\rho_1\omega^2}{E\mu^2}}$ and $\lambda_2 = \sqrt{\dfrac{16\rho_2\omega^2}{E\mu^2}}$ are the single-valued

115   function of eigenfrequency. ρ_2 is the wood density and ρ_1 is the equivalent density regarding the

116   contribution of both tree trunk and crown. Same to A_1-A_4, B_1-B_4 are also coefficients of the tree deflection

117   equation that need to be determined based on the boundary and continuity conditions.

118   The boundary condition at the origin (z=0) is the free end, and thus Eq. 4 can be simplified as:

119
$$u_1(z) = \frac{1}{z}\left[A_1 J_2\left(2\sqrt{\lambda_1 z}\right) + A_3 J_2\left(2i\sqrt{\lambda_1 z}\right)\right] \qquad 0 \leq z < l \qquad (6)$$

120   According to continuity conditions of two segments at the splitting point and the boundary condition

121   at the tree base, following constraints are determined: $u_1(l) = u_2(l)$, $u_1'(l) = u_2'(l)$, $u_1''(l) = u_2''(l)$,

122      $u_1'''(l) = u_2'''(l)$, $u_2(h) = 0$, and $Ku_2'(h) + EI(h)u_2''(h) = 0$. Introducing the constraints into Eqs. (5-6), a total

123   of six equations are determined here. These six equations can be written in a matrix format:

124
$$\left[F\left(\lambda_1, \lambda_2\right)\right]_{6\times6} \cdot \left[A_1 \quad A_3 \quad B_1 \quad B_2 \quad B_3 \quad B_4\right]^T = 0 \qquad (7)$$

125   where $\left[\mathbf{F}\left(\lambda_1, \lambda_2\right)\right]_{6\times6}$ is a matrix that is composed of λ_1 and λ_2 . The orders of eigenfrequency and the

126   corresponding vibration mode can be obtained by solving the equation: the determinant of matric

127      $\left|F(\lambda_1, \lambda_2)\right| = 0$. Notably, the derivatives of $u_1(z)$ and $u_2(z)$ have very complicated expressions but could

128   be easily calculated using Matlab. Therefore, we did not provide the complete expression here.

129   *2.2 Tree motion*

130   The mechanical response of trees subject to an air blast is modeled using a modified multi-degree-of-

131   freedom tree swaying model with variable cross-sections (Zhuang et al., 2022b). Different from the

132   simplification in the eigenfrequency prediction method, the size of tree crown here is determined based

133   on real tree data, corresponding to the frontal area distribution of the tree crown (Fig. 3(a)). The model

134   divides the tree beam into a set of segments and calculates the tree motion using linear modal analysis.

135   Specifically, the tree deformation is deposed into a set of vibration modes so that the total displacement

136   is the combined contribution of each mode. According to preliminary research performed by Sellier et al.

137 (2008) and Pivato et al. (2014), the contribution of the first vibration model is far ahead of the other

138 modes for trees with a slender shape. Thus, only the first vibration mode and the corresponding

139 eigenfrequency are utilized in this study. The modeling of air blast pressure accounts for the wind-tree

140 relative motion and large tree deflection by regarding the beam velocity and geometric nonlinearities

141 resulting from the inclination of beam segments relative to the wind direction (θ_i) (Fig. 3(b)). With

142 respect to the large tree deflection, we also introduce the impact of eccentric gravity into the model,

143 which contributes a lot during the interaction with a powerful air blast. The gravity and wind load acting

144 on each segment can be easily calculated based on the predetermined diameter and frontal area

145 distribution (Fig. 3(a)). Considering that trees often fall in the direction of landslide motion and have

146 little time to sway, the maximum response of the tree is assumed to be reached before the damping forces

147 act (Bartelt et al., 2018). Only the undamped response to a short-duration blast is considered. The tree

148 motion equations and the expression of air blast force are as follows:

$$m\frac{\partial^2 y}{\partial t^2} + ky = \int_0^h F_i \phi \, \mathrm{d}s + \int_0^h G_i \phi \, \mathrm{d}s \qquad (8)$$

$$F_i = 0.5\rho C_\mathrm{d} A_\mathrm{f} \left| v\cos\theta_i - \frac{\partial y}{\partial t}\cos\theta_i \right| \left(v\cos\theta_i - \frac{\partial y}{\partial t}\cos\theta_i \right)\cos\theta_i \qquad (9)$$

$$G_i = m_i g \cdot \sin\theta_i \cdot \cos\theta_i \qquad (10)$$

152 where ϕ, w, $\ m = \int_0^h \overline{m}\phi^2 \mathrm{d}s$, $k = 4\pi^2 m\omega^2$ are the first mode shape, the first eigenfrequency, modal mass

153 and stiffness, respectively, $\overline{m}$ is the mass distribution, y is the associated generalized displacement, F_i

154 and G_i are the air blast loading and eccentric beam gravity act on the ith segment, h is the tree height, C_d

155 is the drag efficient, A_f is the frontal area, ρ and v are the density and velocity of the air blast, respectively.

156 Our model is applicable of calculating the scenarios for both full-height and part-height air blasts.

157   In this study, the air blast velocity is expressed as a sine wave impulse with a short duration time t_0:

$$v = v_\mathrm{max}\sqrt{\sin \varpi t} \qquad (11)$$

159   where $v_{\max}$ is the maximum velocity of the landslide-induced air blast and ϖ can be regarded as the

160   circular frequency of the wind force $\varpi = \pi / t_0$ (wind force is related to the square of its velocity).

161   The mechanical response of trees subject to an air blast is deduced by introducing the calculated

162   wind velocity from Eq. 11 into the tree motion model (Eqs. 8-9), and subsequently solving the equations

163   using the central finite-difference scheme. The validity of this tree motion model has been checked by

164   Pivato et al. (2014) and Zhuang et al. (2022), and thus the validation process is not involved here.

165
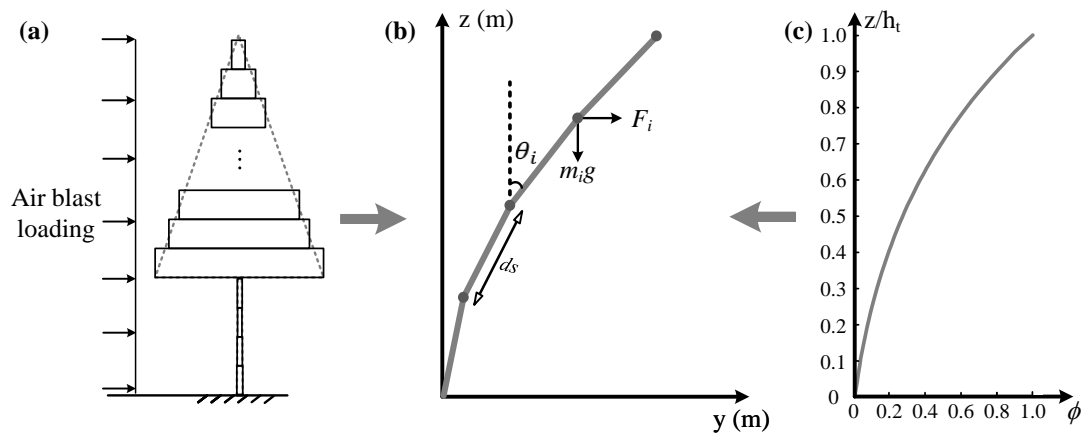
166   **Fig. 3** a-b Modeling the tree as a multi-degree-of-freedom flexible beam to calculate the dynamic
167   response of trees submitted a powerful air blast. c The first mode shape of the beam helps to model the
168   tree deformation.

169   *2.3 Tree breakage*

170   Two failure modes commonly caused by air blasts are involved in the work: bending and overturning

171   (Gardiner et al., 2000).

172   For the case of tree bending, trees are considered to break when the maximum bending stress $\sigma_{\max}$

173   exceeds a critical value σ_{crit} :

174
$$\sigma_{\max} = \left[\frac{M(t,z) \cdot d(z)/2}{I(z)} \right]_{\max} \geq \sigma_{\mathrm{crit}} \tag{12}$$

175   where σ_{crit} is the bending strength of the tree, which depends highly on the material property. $M(t,z)$ is

176   the bending moment, and its value is calculated at each time step all along the beam:

177
$$M(t,z) = EI(z)\frac{\mathrm{d}\theta}{\mathrm{ds}} \tag{13}$$

178 where $\dfrac{\mathrm{d}\theta}{\mathrm{d}s}$ represents the local beam curvature and θ is the angle between the beam segment with the

179 vertical direction.

180 For the tree overturning case, trees are regarded to break at the basement when the air blast-induced

181 moment reaches the anchorage resistance (M_{crit}):

182
$$M_{\text{base}}(t) \geq M_{\text{crit}} \tag{14}$$

183 where $M_{\text{base}}(t)$ is the moment at tree base calculated at each time step, and the anchorage resistance M_{crit}

184 is often determined based on in-situ tests (e.g. tree pulling tests).

185 **3. Application**

186 To demonstrate the power of air blasts and how they damage trees, we consider the problem proposed

187 by Bartelt et al. (2018): a landslide-induced air blast enters a spruce forest at high speed (maximum

188 velocity of 20 m/s). The short-duration air blast lasts a few seconds with a frequency ϖ . Trees in the

189 forest have a height between 25 and 30 m, which is also the height of the air blast. The sliding mass has

190 stopped before reaching the forest and only the air blast loads on the trees.

191 **Table 1** Model parameters used in the numerical simulations of the tree response. Parameters are derived
192 from data contained in Kantola and Mäkelä (2004) and Bartelt et al. (2018).

Height h(m)	Crown height l(m)	Crown width w(m)	Diameter at trunk base D(m)	Wood density ρ_2 (kg/m³)	Branch mass m(kg)	Drag coefficient C_{d}
27	18	5	0.4	480	540	0.4

193 Using the measured biomass parameters presented in Table 1, we set the total crown mass of a single

194 tree to be 540 kg. The tree crown is assumed to be a cone with a length of 18 m ($\dfrac{2}{3}h$) and a width of 5

195 m. The wood density is 480 kg/m³ and the elastic modulus is 10 GPa. Measurements of root anchorage

196 stiffness (K) are very rare and in-situ tests on spruce performed by Neild and Wood (1999) show a value

197 variation of 80-1200 kN·m. This value range indicates a large variation in K depending on the growth

198 conditions, and the values of 100-1200 kN·m are applied in the prediction of eigenfrequency and

199   vibration mode in this study.

200   The eigenfrequency ranging from 0.13 Hz (K=100 kN·m) to 0.32 Hz (K=1200 kN·m) is calculated

201   based on the above parameters (Fig. 4). The modeled results are in high agreement with measurements

202   performed by Jonsson et al. (2006) (0.16-0.30 Hz), indicating the validity of our proposed eigenfrequency

203   prediction method. Although the tree eigenfrequency varies significantly with the anchorage stiffness, all

204   the calculated values are less than 0.5 Hz. The same order of magnitude between tree eigenfrequency

205   and air blast frequency necessitates a further investigation on the possible impact of resonance. The

206   dynamic magnification effect caused by impulse loading can greatly amplify the static stress state,

207   making the trees easier to be damage.

208
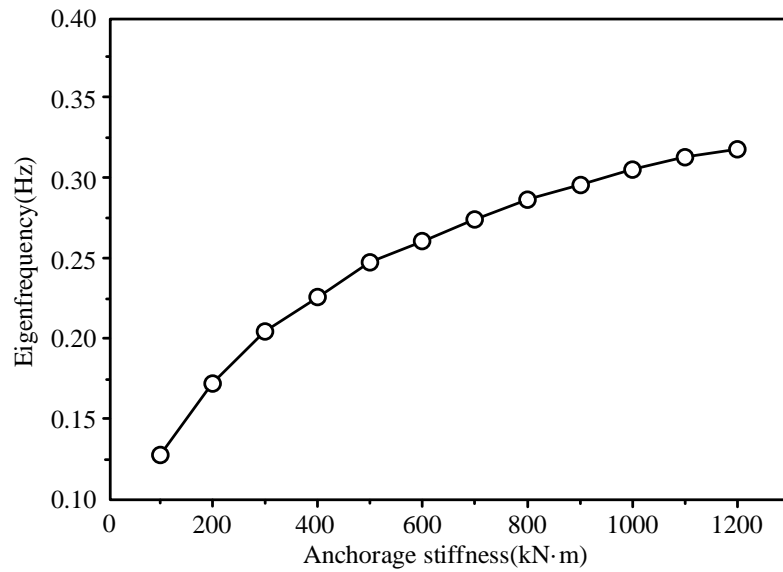
209   **Fig. 4** Eigenfrequency of trees corresponding to different anchorage stiffness.

210   To investigate the impact of dynamic magnification, we performed simulations for all the scenarios

211   using the tree eigenfrequency of 0.26 Hz (K=600 kN·m) and the associated vibration mode. A

212   magnification factor D is defined to describe this effect:

213
$$D = \frac{u_{\mathrm{d,max}}(\beta)}{u_{\mathrm{sta}}} = \frac{u_{\mathrm{d,max}}(\beta)}{\int_0^h F_{\mathrm{s,max}} \phi \mathrm{d}s / k} = \frac{u_{\mathrm{d,max}}(\beta)}{\int_0^h \rho C_{\mathrm{d}} A_{\mathrm{f}} v_{\max}^2 \phi \mathrm{d}s / k} \tag{15}$$

214   where $u_{\mathrm{d,max}}$ and u_{sta} are the maximum displacement subject to dynamic load and static load, respectively,

215    $F_{\text{s,max}}$ is the static wind force corresponding to the maximum air blast velocity and $\beta = \dfrac{\varpi}{\omega}$ is the ratio

216   between the air blast frequency (ϖ) and the eigenfrequency of the tree (ω). Notably, the air blast is a

217   multi-medium fluid that contains numerous dusts, showing a higher density than air. Measurements and

218   numerical modeling performed by Swiss researchers (Feistl et al., 2015) suggest $\rho = 5\,\text{kg}/\text{m}^3$. In this

219   scenario u_{sta} is calculated to be 9.8 m.

220
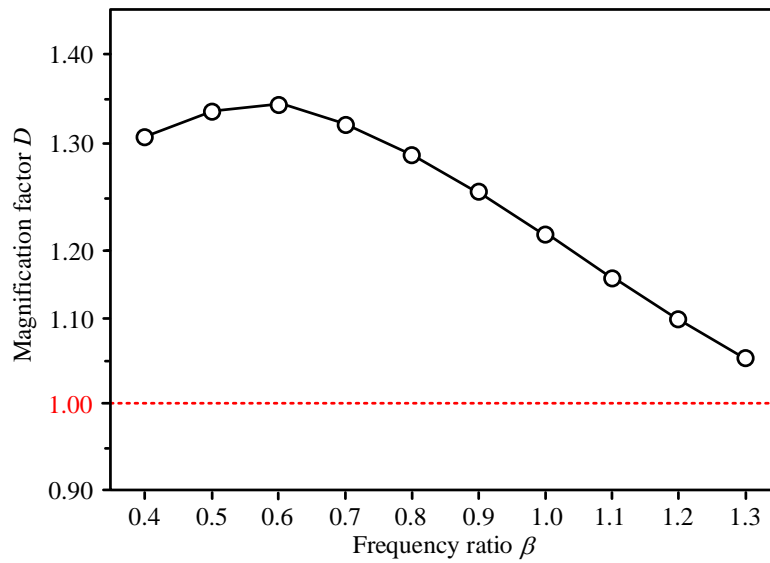
221   **Fig. 5** Magnification factor with various frequency ratio.

222   Fig. 5 shows the impact of air blast frequency on the dynamic magnification effect. A parabola

223   relationship is identified between the magnification factor and the frequency ratio. Consider first an

224   impulse air blast lasting 1.6 s ($\beta = 1.2$). The air blast frequency is higher than that of the tree, implying

225   the maximum displacement reaches after the loading time. The modeled maximum dynamic deformation

226    $u_{\text{d,max}}$ reaches 10.7 m, and the magnification factor is 1.09. In this case, the magnification effect of tree

227   deformation seems not significant because of the large tree deflection and short-duration loading, and

228   the modeled result is similar to the static stress state. For a longer air blast duration of 3.2 s ($\beta = 0.6$), we

229   find D=1.34, a high value. The maximum tree deformation reaches during the air blast loading. In such

230   a scenario, an air blast travelling at 20 m/s can exert similar destruction as a long-duration wind moves

231   at 25 m/s. The dynamic magnification effect significantly increases the tree displacement and thus causes

232   such a phenomenon. Measurements of air blast duration reported by Russian and Swiss researchers

233   (Grigoryan et al., 1982; Sukhanov, 1982) are within this range, lasting only a few seconds. Although the

234   large tree deflection decreases the wind loading, the impulse air blast load is prone to damage the trees

235   because of the dynamic magnification effect.

236   Additional simulations were performed on the air blast induced-tree breakage. The impulse air blast

237   is assumed to have a maximum velocity of 20 m/s and a duration of 3.2 s. For this case, numerical results

238   demonstrate the maximum bending stress and moment of 35 Mpa and 192 kN·m, respectively. The

239   maximum bending stress reaches at 9 m height ($1/3h$), and the maximum bending moment is identified

240   at the tree base. In natural forest areas, the bending strength σ_{crit} and anchorage resistance M_{crit} are highly

241   variable, depending on tree species, soil characteristics and temperatures, etc. Measurements conducted

242   by Peltola et al. (2000) and Lundström et al. (2007) indicate that the bending stress to destroy mature

243   trees needs to exceed a value of 30 MPa while mature spruces with a height of 20-40 m have an anchorage

244   resistance reaches up to 100-400 kN·m. For the case performed in this study, the forest is likely to damage

245   in both bending and overturning failure modes. Reliable values of critical parameters are needed during

246   the assessment of tree destruction, and this will improve the prediction accuracy of the likely failure

247   mode.

248   A further application was performed on the 2008 Wenjia valley avalanche-induced air blast in

249   Sichuan, China (Fig. 6a). This large avalanche has a volume of over $40\times10^6\,\mathrm{m}^3$ and generated a powerful

250   air blast. According to our previous investigations and numerical modeling (Zhuang et al. 2019), the air

251   blast-damaged trees are mostly tall spruce concentrated near the turning points of the valley (Fig. 6 b-c).

252   The simulated air blast velocity at turning points reaches 30 m/s (point A) and 35 m/s (point B),

respectively. Using the spruce-related parameters indicated in Table 1 and an assumed air blast duration

of 3.2 s (a long duration for large avalanches), the maximum displacement of spruces is calculated to be

18.5 m and 22.2 m at points A and B, respectively. In this case, the maximum bending stress of trees at

two turning points could reach 51 Mpa and 57 Mpa, respectively, significantly larger than the bending

strength suggested by Peltola et al. (2000) (36 Mpa). Therefore, bending failure of tall spruces was widely

identified in situ.
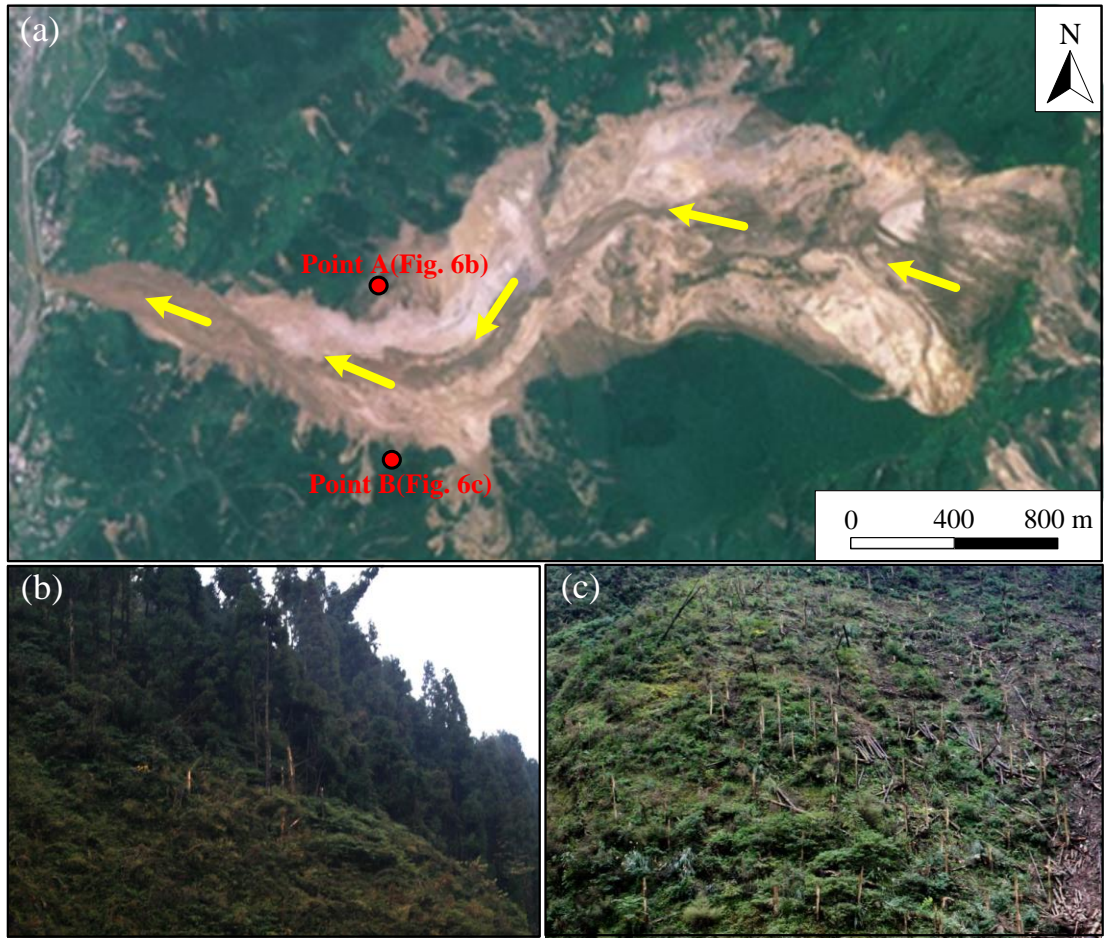
Fig. 6 Wenjia valley avalanche-induced air blast (According to Zhuang et al. 2019). a Overview of the

Wenjia valley avalanche. b-c Trees damaged by the generated air blast.

4. Discussion

Risk assessment and disaster mitigation of landslide-induced air blasts are hot issues in mountainous

regions. Developing a simple but applicable relationship between air blast pressure and tree failure is of

265   great utility for scientists to quantify the air blast power. Compared with existing models, one significant

266   improvement of our model is to model the tree as a flexible beam with variable cross-section and involve

267   the impact of anchorage. This improvement allows the tree to move as its natural vibration mode rather

268   than a hypothetical trajectory (e.g. rotate around the tree base as a rigid body (Bartelt et al., 2018)).

269   Moreover, the variable cross-section makes the modeling of tree bending failures more realistic. We can

270   simulate the failure position of trees subjected to a powerful air blast. For the existing model with a

271   constant diameter (Feistl et al., 2015), the rigidity EI is constant along the beam, and the maximum

272   bending stress is always identified at the tree base. This failure characteristic cannot match the actual

273   situation well.

274   Our proposed model accounts for the impacts of large tree deflection: eccentric gravity and

275   modeling of air blast force regarding the wind-tree relative motion and geometric nonlinearities. To

276   investigate the impact of these factors and confirm the necessity of considering large deflection, a

277   comparative analysis is needed to make readers have a better understand. Therefore, we designed a

278   comparative analysis by simplifying the tree motion model of Eq. 8 without involving the impact of large

279   tree deflection. The simplified model is similar to that proposed by Bartelt et al. (2018):

$$m\frac{\partial^2 y}{\partial t^2} + ky = \int_0^h 0.5\rho C_d A_f v_{max}^2 \phi ds \cdot \sin \varpi t = \int_0^h F_{s,max} \phi ds \cdot \sin \varpi t \tag{16}$$

281   The displacement at the tree top can be written as:

$$\begin{cases} u(t) = \dfrac{\int_0^h F_{s,max}\phi ds}{k} \dfrac{1}{1-\beta^2}(\sin \varpi t - \beta \sin \omega t) & 0 \le t \le t_0 \\ u(t) = \dfrac{u'(t_0)}{\omega}\sin \omega(t-t_0) + u(t_0)\cos \omega(t-t_0) & t > t_0 \end{cases} \tag{17}$$

283   The maximum deformation occurs during the loading time when $\beta \le 1$, and after the loading time

284   when $\beta > 1$. The magnification factor D for both scenarios can be expressed as:

285

$$\begin{cases} D = \dfrac{1}{1-\beta^2}[\sin(\dfrac{2\pi\beta}{\beta+1}) - \beta\sin\dfrac{2\pi}{\beta+1}] & \beta \leq 1 \\[3mm] D = \dfrac{2\beta}{\beta^2-1}\cos\dfrac{\pi}{2\beta} & \beta > 1 \end{cases} \tag{18}$$
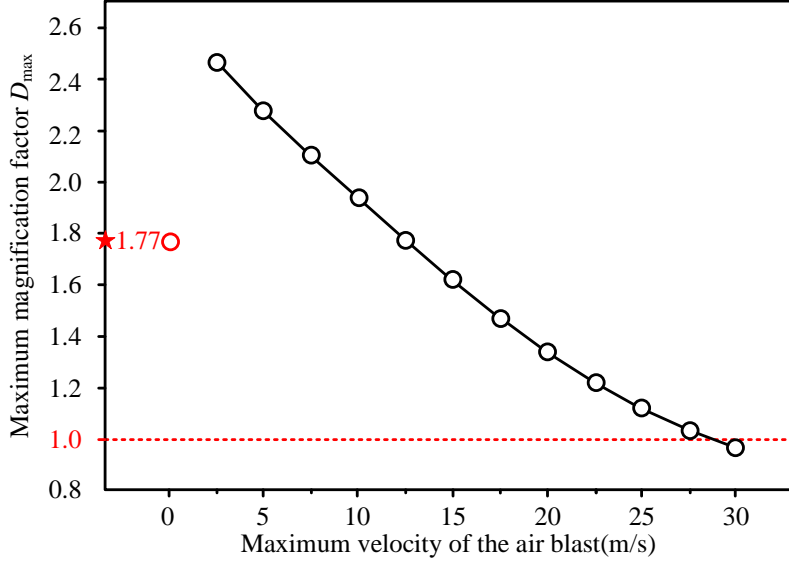
286

287 **Fig. 7** Impact of large tree deflection on the maximum magnification factor D_{max}. The red star represents

288 the D_{max} calculated from Eq. 18. The red circle represents the D_{max} corresponding to the scenario with a

289 very low air blast velocity (maximum velocity of 0.1m/s) and the eccentric gravity is not considered.

290   Fig. 7 presents the impact of large tree deflection on the magnification effect. We first perform the

291 simulation using the proposed model without regarding the impact of large tree deflection. A very low

292 air blast velocity (maximum velocity of 0.1m/s) is performed and the eccentric gravity is not considered.

293 The D_{max} value of 1.77 is identified in the scenario, which is consistent with the analytical solution from

294 Eq. 18. The tree deformation is small with such a weak air blast loading, and the comparison result

295 verifies the validity of our proposed model. Further calculations with higher air blast velocities show

296 different results. In the cases of a low air blast velocity, the eccentric gravity contributes a lot to the tree

297 deformation, causing a rather large magnification factor (>2). However, D_{max} greatly decreases with the

298 increase of wind velocity. For a high air blast velocity, the dynamic response and eccentric gravity

299 amplify the tree deflection, but the inclination of the trees to the wind direction significantly reduces the

300 air blast loading. This special mechanism was rarely considered during the previous assessment of

301 landslide-induced air blasts. We suggest that the modeled tree deformation subjected to a powerful air

302 blast might be overestimated without considering large tree deflection, although this simplified model of

303 Eq. 18 has the advantage of rapid assessment for air blast pressure. The impact of large tree deflection

304 should be accounted for when using forest destruction to quantify the air blast danger.

305   The dynamic response of trees subject to a landslide-induced air blast is a complex problem,

306 depending heavily on the biometric characteristics of trees. Some biomass variations can be represented

307 by the parameters in the proposed model. For example, for the leafless trees, air blasts pass through the

308 tree crown and only act on the branches, causing a smaller wind load. A reduction of drag efficient C_d is

309 needed in such a condition. Single trees in the impact region of air blasts are subject to a larger loading

310 than trees in dense forest stands, where tree crowns tend to be narrower and form a shielding effect. We

311 can make a reduction in the frontal area A_f to simulate this mechanism. Furthermore, although much

312 effort has been paid to the biometric and mechanical characteristics of tree crowns and trunks, less

313 information is available about the anchorage stiffness and resistance. The root anchorage properties

314 significantly influence the tree eigenfrequency and the likely failure mode. A reliable measurement value

315 of tree bending strength and anchorage resistance is of utility to improve the accuracy of tree failure

316 prediction and clarify which failure mode is prone to occur. Overall, biomass-related parameters selected

317 to estimate the air blast pressure are recommended to be determined based on in-situ investigations. In

318 the future, more measurements need to be conducted on the anchorage properties of trees. Regional

319 databases for biometric and mechanical properties of trees are worthwhile to be established. This would

320 help provide reliable parameters for the air blast risk assessment.

321   In this study, the tree is modeled as a variable cross-section that is hinged at ground level using

322 elastic support. Root anchorage is complex and sensitive to many factors such as soil mechanical

323   properties, soil water content and root morphology, and we acknowledge that it is difficult to establish a

324   model that accounts for all the factors that affect the anchorage. Most importantly, we developed a simple

325   but practical model that could simulate the dynamic response of trees subject to a powerful air blast and

326   their two possible failure modes. Bartelt and his colleagues (Bartetl et al., 2018) have developed a

327   dynamic model named RAMMS, which could efficiently model the entire movement process of

328   ice/rock/snow avalanches and the associated air blasts. It is anticipated that the combination of our

329   proposed tree model and the RAMMS dynamic model could help the risk assessment of potential air

330   blasts through modeling the air blast impact region and forest destruction.

331   **Conclusions**

332   Air blasts are short-duration impulses and can intensity the potential destruction far beyond the sliding

333   mass. Trees destruction in-situ can provide valuable data to quantify the air blast danger and make us

334   better understand its force of destruction. In this study, we developed a framework for the forest

335   destruction assessment subject to a powerful air blast, including the eigenfrequency prediction method,

336   tree motion equations and breakage conditions. The tree is modeled as a flexible variable cross-section

337   beam hinged at ground using elastic support. The impacts of root anchorage and large tree deflection are

338   regarded during the dynamic response analysis. The framework also involved two failure modes (bending

339   and overturning) and the corresponding failure criteria so that the risk of forest damage could be assessed.

340   Using the proposed framework, we assumed conditions to investigate the air blast power. Modeling

341   results demonstrate that although the anchorage properties significantly influence the tree eigenfrequency,

342   the tree eigenfrequency is always in the same order as air blast frequency. The associated dynamic

343   magnification effect amplifies the tree deformation and thus makes the tree damage easier. In the scenario

344   with a similar frequency between air blasts and trees, an air blast travelling at 20 m/s causes a similar

force of destruction as a long-duration wind load moves at 25 m/s. Notably, this magnification effect

caused by the dynamic response and eccentric gravity is significant in the cases of low wind velocity,

while the large tree deflection caused by strong air blast loading would weaken this effect. Furthermore,

bending and overturning are two likely failure modes for trees subject to a powerful air blast, but exactly

what kind of failure will occur for a specific forest depends heavily on the properties of both trees and

soil. A case application was further performed on the 2008 Wenjia valley avalanche-induced air blast in

China, checking the validity of our proposed model. In the future, more measurements should be

conducted on biometric and mechanical properties of trees, and a regional parameter database is

worthwhile to be established. This would greatly improve the prediction accuracy of tree damage and air

blast pressure.

Data availability

No data sets were used in this article.

Author contribution

Yu Zhuang did the numerical work and wrote the manuscript with contributions from all co-authors.

Aiguo Xing and Perry Bartelt designed the work and modified the manuscript. Bilal Muhammad

evaluated the results and proposed various improvements that were incorporated. Zhaowei Ding helped

with the eigenfrequency prediction model.

Competing interest

The authors declare that they have no known competing financial interests or personal relationships that

could have appeared to influence the work reported in this paper.

Acknowledgments

This study was supported by the National Natural Science Foundation of China (No. 41977215).

367 **References**

368 Adams, J.: Earthquake-dammed lakes in New Zealand, Geology, 9, 215-219, 1881.

369 Bartelt, P., and Stöckli, V.: The influence of tree and branch fracture, overturning and debris entrainment

370   on snow avalanche flow, Annals of Glaciology, 32, 209-216, 2001.

371 Bartelt, P., Buser, O., Vera Valero, C., and Bühler, Y.: Configurational energy and the formation of mixed

372   flowing/powder snow and ice avalanches, Annals of Glaciology, 57(71), 179-188, 2016.

373 Bartelt, P., Bebi, P., Feistl, T., Buser, O., and Caviezel, A.: Dynamic magnification factors for tree blow-

374   down by powder snow avalanche air blasts, Natural Hazards Earth System Sciences, 18, 759-764,

375   2018.

376 Bartelt, P., Christen, M., Bühler, Y., and Buser, O.: Thermomechanical modelling of rock avalanches with

377   debris, ice and snow entrainment, Numerical Methods in Geotechnical Engineering IX, Taylor &

378   Francis Group, London, pp 1047-1054, 2018.

379 Caviezel, A., Margreth, S., Ivanova, K., Sovilla, B., and Bartelt, P.: Powder snow impact of tall vibrating

380   structures, Eccomas Proceedia Compdyn, 5318-5330, 2021.

381 Feistl, T., Bebi, P., Christen, M., Margreth, S., Diefenbach, L., and Bartelt, P.: Forest damage and snow

382   avalanche flow regime, Natural Hazards and Earth System Sciences, 15, 1275-1288, 2015.

383 Fujita, K., Inoue, H., Izumi, T., Yamaguchi, S., Sadakane, A., Sunako, S., Nishimura, K., Immerzeel, W.

384   W., Shea, J. M., Kayastha, R. B., Sawagaki, T., Breashears, D. F., Yagi, H., and Sakai, A.:

385   Anomalous winter-snow-amplified earthquake-induced disaster of the 2015 Langtang avalanche in

386   Nepal, Natural Hazards Earth System Sciences, 17, 749-764, 2017.

387 Gardiner, B., Peltola, H., and Kellomäki, S.: Comparison of two models for predicting the critical wind

388   speeds required to damage coniferous trees, Ecological Modelling, 129, 1-23, 2000.

389   Grigoryan, S., Urubayev, N., and Nekrasov, I.: Experimental investigation of an avalanche air blast, Data

390   Glaciology Student, 44, 87-93, 1982.

391   Jonsson, M. J., Foetzki, A., Kalberer, M., Lundström, T., Ammann, W., and Stöckli, V.: Root-soil rotation

392   stiffness of norway spruce (Picea abies (L.) Karst) growing on subalpine forested slopes, Plant Soil,

393   285, 267-277, 2006.

394   Johnson, B. C., and Campbell, C. S.: Long-runout landslides are among the most spectacular and

395   catastrophic geologic processes, Geophysical Research Letters, 44(12), 12091-12097, 2017.

396   Kantola, A., and Mäkelä, A.: Crown development in Norway spruce [Picea abies(L.) Karst.], Trees, 18,

397   408-421, 2004.

398   Kargel JS, et al. (2016) Geomorphic and geologic controls of geohazards induced by Nepal's 2015

399   Gorkha earthquake. Science, 351, aac8353.

400   Keshmiri, A., Wu, N., and Wang, Q.: Free Vibration Analysis of a Nonlinearly Tapered Cone Beam by

401   Adomian Decomposition Method, International Journal of Structural Stability and Dynamics, 18(7),

402   1850101, 2018.

403   Lundström, T., Jonsson, M. J., and Kalberer, M. The root-soil system of Norway spruce subjected to

404   turning moment: resistance as a function of rotation, Plant Soil, 300, 35-49, 2007.

405   Mocica, G.: Special Functions Problems, Bucharest: Didactic and Pedagogic Publishing House, 1988.

406   Neild, A. S., and Wood, C. J.: Estimating stem and root-anchorage flexibility in trees, Tree Physiology,

407   19, 141-151, 1999.

408   Nicoll, B. C., Gardiner, B. A., Rayner, B., Peace, A. J.: Anchorage of coniferous trees in relation to

409   species, soil type, and rooting depth, Canadian Journal of Forest Research, 36, 1871-1883, 2006.

410   Penna, I. M., Hermanns, R. L., Nicolet, P., Morken, O. A., and Jaboyedoff, M.: Airblasts caused by large

slope collapses, Geological Society of America Bulletin, 133, 939-948, 2021.

Peltola, H., Kellomäki, S., Väisänen, H., and Ikonen, V.: A mechanistic model for assessing the risk of wind and snow damage to single trees and stands of scots pine, norway spruce, and birch, Canadian Journal of Forest Research, 29, 647-661, 1999.

Peltola, H., Kellomäki, S., Hassinen, A., and Granander, M.: Mechanical stability of Scots pine, Norway spruce and birch: an analysis of tree-pulling experiments in Finland, Forest Ecology and Management, 135, 143-153, 2000.

Pivato, D., Dupont, S., and Brunet, Y.: A simple tree swaying model for forest motion in windstorm conditions, Trees, 28, 281-293, 2014.

Sellier, D., Brunet, Y., and Fourcaud, T.: A numerical model of tree aerodynamic response to a turbulent airflow, Forestry, 81(3), 279-297, 2008.

Shugar, DH. et al.: A massive rock and ice avalanche caused the 2021 disaster at Chamoli, Indian Himalaya, Science, 373(6552), 300-306, 2021.

Šilhán, K.: Tree ring evidence of slope movements preceding catastrophic landslides, Landslides, 17, 615-626, 2020.

Sukhanov, G.: The mechanism of avalanche air blast formation as derived from field measurements, Data Glaciology Student, 44, 94-98, 1982.

Yin, Y. P., and Xing, A. G.: Aerodynamic modeling of the yigong gigantic rock slide-debris avalanche, Tibet, China. Bulletin of Engineering Geology and the Environment, 71, 149-160, 2012.

Yin, Y. P.: Vertical acceleration effect on landsides triggered by the Wenchuan earthquake, China. Environmental Earth Sciences, 71, 4703-4714, 2014.

Zhuang, Y., Xu, Q., and Xing, A. G.: Numerical investigation of the air blast generated by the Wenjia

433   valley rock avalanche in Mianzhu, Sichuan, China, Landslides, 16, 2499-2508, 2019.

434   Zhuang, Y., Xu, Q., Xing, A. G., Bilal, M., Gnyawali, K. R. (2022) Catastrophic air blasts triggered by

435   large ice/rock avalanches, Landslides, 2022. Doi: 10.1007/s10346-022-01967-8.

436   Zhuang, Y., Xing, A. G., Jiang, Y. H., Sun, Q., Yan, J. K., and Zhang, Y. B.: Typhoon, rainfall and trees

437   jointly cause landslides in coastal regions, Engineering Geology, 298, 106561, 2022b.